



Advanced mapping strategies for ablation therapy in adults with congenital heart disease

Fares-Alexander Alken^{1,2}, Niklas Klatt¹, Paula Muenkler^{1,2}, Katharina Scherschel^{1,2}, Christiane Jungen^{1,2}, Ruken Oezge Akbulak¹, Ann-Kathrin Kahle^{1,2}, Melanie Gunawardene¹, Mario Jularic¹, Leon Dinshaw¹, Jens Hartmann¹, Christian Eickholt^{1,2}, Stephan Willems^{1,2}, Fridrike Stute³, Goetz Mueller³, Stefan Blankenberg^{2,4}, Carsten Rickers^{3,5}, Christoph Sinning⁴, Elvin Zengin-Sahm⁴, Christian Meyer^{1,2}

¹Department of Cardiology-Electrophysiology, cNEP, Cardiac Neuro- and Electrophysiology Research Group, University Heart Center, University Hospital Hamburg-Eppendorf, Martinistrasse 52, 20246 Hamburg, Germany; ²DZHK (German Center for Cardiovascular Research), Partner Site Hamburg/Kiel/Lübeck, Hamburg, Germany; ³Department of Pediatric Cardiology/Pediatric Cardiac Surgery, ⁴Department of General and Interventional Cardiology, ⁵Adults with Congenital Heart Disease Section, University Heart Center, University Hospital Hamburg-Eppendorf, Martinistrasse 52, 20246 Hamburg, Germany

Contributions: (I) Conception and design: FA Alken, C Meyer; (II) Administrative support: S Blankenberg, E Zengin-Sahm, C Rickers, C Meyer, S Willems; (III) Provision of study materials or patients: N Klatt, P Muenkler, M Gunawardene, M Jularic, L Dinshaw, J Hartmann, RO Akbulak, C Eickholt; (IV) Collection and assembly of data: C Sinning; (V) Data analysis and interpretation: AK Kahle, FA Alken; (VI) Manuscript writing: All authors; (VII) Final approval of manuscript: All authors.

Correspondence to: Christian Meyer, MD, MA. Department of Cardiology-Electrophysiology, University Hospital Hamburg, University Heart Center, Martinistrasse 52, 20246 Hamburg, Germany. Email: c.mey@web.de.

Background: Ultra-high density mapping (HDM) is a promising tool in the treatment of patients with complex arrhythmias. In adults with congenital heart disease (CHD), rhythm disorders are among the most common complications but catheter ablation can be challenging due to heterogenous anatomy and complex arrhythmogenic substrates. Here, we describe our initial experience using HDM in conjunction with novel automated annotation algorithms in patients with moderate to great CHD complexity.

Methods: We studied a series of consecutive adult patients with moderate to great CHD complexity and an indication for catheter ablation due to symptomatic arrhythmia. HDM was conducted using the Rhythmia™ mapping system and a 64-electrode mini-basket catheter for identification of anatomy, voltage, activation pattern and critical areas of arrhythmia for ablation guidance. To investigate novel advanced mapping strategies, postprocedural signal processing using the Lumipoint™ software was applied.

Results: In 19 patients (53±3 years; 53% male), 21 consecutive ablation procedures were conducted. Procedures included ablation of atrial fibrillation (n=7; 33%), atrial tachycardia (n=11; 52%), atrioventricular accessory pathway (n=1; 5%), the atrioventricular node (n=1; 5%) and ventricular arrhythmias (n=4; 19%). A total of 23 supraventricular and 8 ventricular arrhythmias were studied with the generation of 56 complete high density maps (atrial n=43; ventricular n=11, coronary sinus n=2) and an average of 12,043±1,679 mapping points. Multiple arrhythmias were observed in n=7 procedures (33% of procedures; range of arrhythmias detected 2–4). A total range of 1–4 critical areas were defined per procedure and treated within a radiofrequency application time of 16 (interquartile range 12–45) minutes. Postprocedural signal processing using Lumipoint™ allowed rapid annotation of fractionated signals within specific windows of interest. This supported identification of a practical critical isthmus in 20 out of 27 completed atrial and ventricular tachycardia activation maps.

Conclusions: Our findings suggest that HDM in conjunction with novel automated annotation algorithms provides detailed insights into arrhythmia mechanisms and might facilitate tailored catheter ablation in patients with moderate to great CHD complexity.

Keywords: Congenital heart disease (CHD); arrhythmia; atrial fibrillation; ventricular tachycardia; atrial tachycardia; catheter ablation

Submitted Apr 10, 2019. Accepted for publication Oct 01, 2019.

doi: 10.21037/cdt.2019.10.02

View this article at: <http://dx.doi.org/10.21037/cdt.2019.10.02>

Introduction

The population of patients with congenital heart disease (CHD) is continuously increasing as today about 90% of patients reach adulthood due to improved therapeutic options (1). Approximately half of these patients are expected to experience arrhythmias because of the underlying congenital heart defect itself or as a sequela of interventional or surgical treatment (1,2). Catheter ablation in this cohort is an important therapeutic option attributable to frequently experienced drug refractoriness and possible hemodynamic deterioration (3,4). Three-dimensional (3D) electroanatomic mapping systems are commonly used in these patients as their role in producing favorable outcome in CHD-related catheter ablation has been demonstrated (5-7). Currently, further technological advances, such as ultra-high density mapping (HDM) including multipolar catheters with small electrode size and spacing, are providing further solutions for the various challenges encountered during electrophysiological studies in adult patients with CHD (8-12). However, data reporting on acute ablation outcome in patients with CHD using these novel technologies are sparse (8,12). Therefore, the aim of the present study was to investigate the contribution of HDM in conjunction with novel automated annotation algorithms to the treatment of cardiac arrhythmias in patients with moderate to great CHD complexity.

Methods

Study design and patient selection

The study was approved by the local ethics committee of the University of Hamburg (No. WF-79/16) and informed consent was taken from all patients.

We investigated 19 consecutive adult patients with a history of treated or untreated CHD and an indication for catheter ablation due to symptomatic arrhythmia using the Rhythmia™ mapping system in conjunction with automated annotation algorithms incorporated in the novel Lumipoint™ software (Boston Scientific Corporation, Marlborough, MA, USA). Only patients with CHD of moderate to great complexity were included into the study, according to the ACHD AP classification

including anatomical and physiological criteria defined by the current guidelines of the management of adults with CHD (3). Anatomical abnormalities such as anomalous pulmonary venous connection, congenital aortic valve disease, Ebstein anomaly, ventricular septum defect, supra-valvar aortic stenosis or unrepaired secundum atrial septum defect were considered as CHD of moderate complexity (3). Patients presenting with transposition of the great arteries (TGA), cyanotic CHD, Fontan procedure, interrupted aortic arch, mitral/pulmonary atresia, truncus arteriosus, a single/double-outlet ventricle or other abnormalities of atrioventricular and ventriculoarterial connection were classified as CHD of great complexity (3). Moreover, physiological variables including arrhythmia severity, exercise capacity and end-organ dysfunction were considered for classification (physiological stage A–D), as many have prognostic value in patients with CHD. Patients were classified based on the “highest” relevant anatomic or physiological feature (3).

Electrophysiological study and periprocedural imaging

Prior to ablation, transthoracic and/or transesophageal echocardiography were performed for evaluation of global cardiac function and exclusion of intracardial thrombi. Additional imaging was performed and imported into the HDM system prior to the procedure for better evaluation of complex anatomy if reasonable (*Figure 1*). Patients were under conscious sedation by intravenous propofol and fentanyl administration throughout the procedure (13). Hemodynamic monitoring was conducted by continuous assessment of saturation, non-invasive or invasive blood pressure as well as surface and intracardiac ECG recording. All tracings were recorded and stored on a digital amplifier/recorder system (LabSystem PRO®, Bard Electrophysiology Inc., Lowell, MA, USA). The general catheter setting consisted of the following: (I) a steerable 6F decapolar diagnostic catheter (Inquiry™, 5 mm spacing; St. Jude Medical, Saint Paul, MN, USA) positioned in the coronary sinus and serving as the reference of the Rhythmia™ 3-D electroanatomical mapping system (Boston Scientific Corporation, Marlborough, MA, USA); as for ventricular procedures, an additional 5F quadripolar

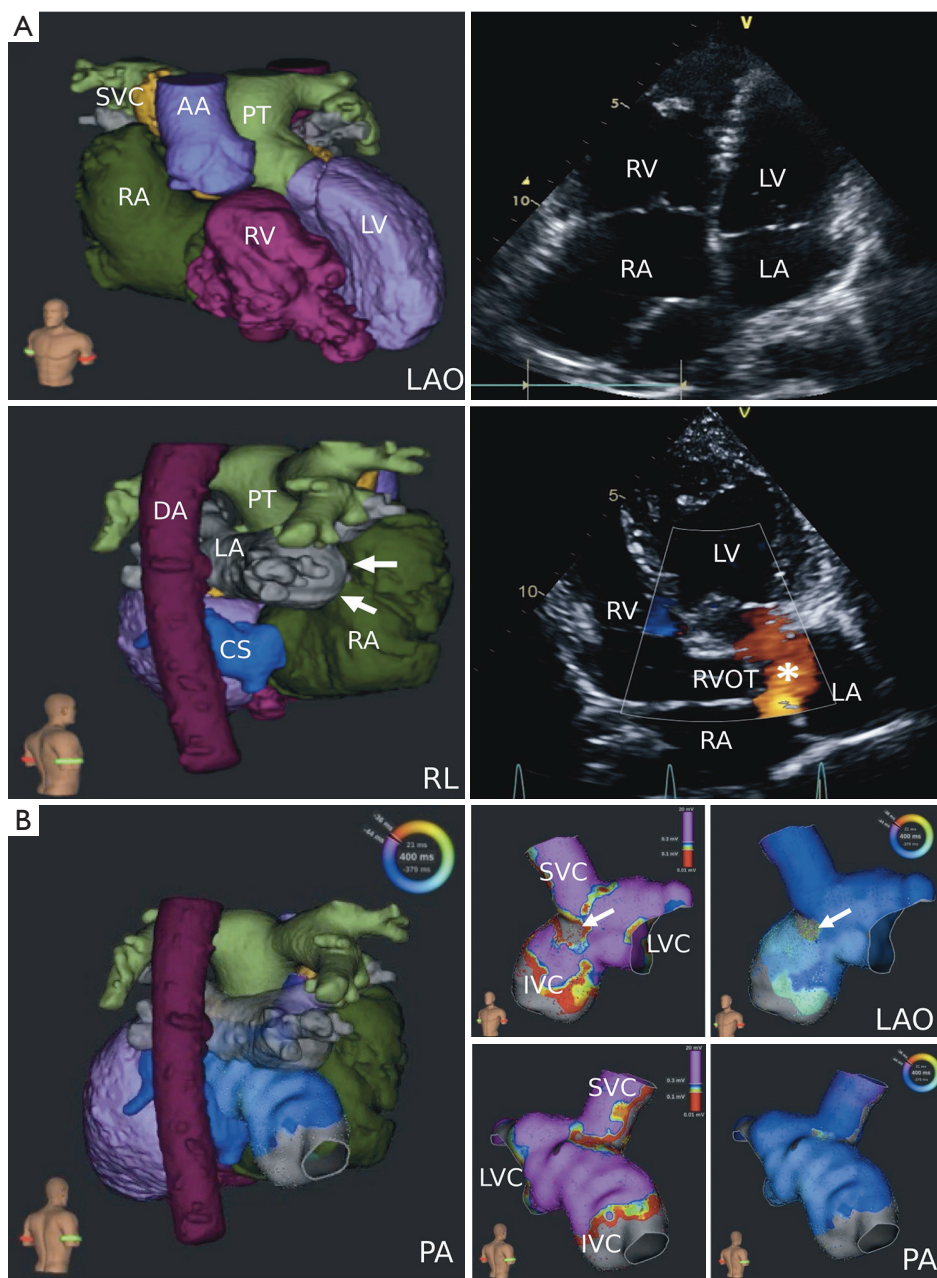


Figure 1 Multimodal imaging in patients with great CHD complexity. (A) Image integration of a computed tomography scan into the HDM system in a patient with transposition of the great arteries, previous Mustard procedure and recurrent atrial tachycardia. The anatomical right ventricle (RV) (upper left figure) is shown, which is connected to the ascending aorta (AA) as the functional systemic ventricle. Echocardiographic imaging (right figures) visualizes the largely dilated right atrium (RA) and RV (upper right figure, apical 4-chamber view) as well as the blood flow inside the baffle (marked the by the white *, lower right figure) from the inferior (IVC) and superior vena cava (SVC) into the systemic venous antrum. RA and left atrium (LA) are connected via a shunt (white arrows, lower left figure), creating a systemic atrium. (B) Voltage and HDM with consecutive integration of maps into the computed tomography scan. The connection of the LV to the SVC and IVC via the baffle (LVC) can be seen. The no voltage/no activation area (upper middle/upper right figure, grey area marked by white arrows) marks the shunt connection between RA and LA. AA, ascending aorta; CS, coronary sinus; DA, descending aorta; IVC, inferior vena cava; LA, left atrium; LAO, left anterior oblique view; LV, left ventricle; PA, posterior-anterior view; LVC, left ventricular connection; PT, pulmonary trunk; LV, left ventricular connection; RA, right atrium; RL, right lateral view; RVOT, right ventricular outflow tract; SVC, superior vena cava.

catheter (IBI Inquiry™; St. Jude Medical) was placed in the right ventricular apex; (II) an expandable, open irrigated 64-pole basket mapping catheter (IntellaMap Orion™, Boston Scientific) comprising of 8 splines with 8 electrodes (electrode spacing 2.5 mm, electrode surface area 0.4 mm²) for atrial as well as ventricular procedures as described elsewhere (14,15); (III) an open-irrigated tip, bidirectional mapping and ablation catheter (IntellaNav MiFi™ OI, Boston Scientific). For pulmonary vein isolation (PVI), catheters were introduced into the left atrium by double transseptal access using a fixed curve long sheath (SL0, 8-F; St. Jude Medical, for ablation catheter) and a long steerable sheath (Zurpaz™, medium curl, 8.5-F, Boston Scientific, for mini basket catheter). Intravenous heparin administration and continuous activated clotting time monitoring were conducted after first access of the left atrium or after introduction of the basket catheter into any chamber of the heart to maintain an activated clotting time >300 seconds.

Ultra-high density 3-D mapping

HDM of the cardiac chambers was performed with the basket catheter acquiring data during sinus rhythm, during pacing from the coronary sinus and/or during ongoing arrhythmia. If patients were in sinus rhythm at the beginning of the procedure, arrhythmias were induced by burst pacing or programmed stimulation. Electrogram annotation was performed automatically by the mapping system using the following criteria for beat acceptance: (I) cycle length stability: ± 10 ms; (II) stability of relative timing of reference electrograms: ± 5 ms; (III) respiration gating: automatic measurement and filtering of motion above maximum inspiration movement by change of impedance of the ECG-electrodes; (IV) electrode location stability (catheter stability): 2–3 mm. A detailed description of the systems electrogram annotation has been published before (16). Maps were considered complete when the entire chamber anatomy was reconstructed with the best achievable electrode-tissue contact. Complete activation maps of macroreentrant supraventricular tachycardia or ventricular tachycardia (VT) were defined as mapping of $\geq 90\%$ of the cycle length. If necessary, additional mapping was performed at the operator's discretion using the ablation catheter.

Catheter ablation

Radiofrequency current was applied with a maximum power

of 30–40 W and an irrigation rate of 17–30 mL/min for up to 120 seconds not exceeding an upper temperature limit of 48 °C. The energy level was reduced to 20–25 W at the posterior left atrium wall. After restoration of sinus rhythm, pacing maneuvers and pharmacological arrhythmia provocation were repeatedly performed to test for non-inducibility of arrhythmias until atrial refractoriness or 200 ms cycle length were reached. A bidirectional block was confirmed whenever linear lesions were generated and additional activation mapping was performed if necessary (17). When indicated, PVI or cavotricuspid isthmus (CTI) ablation was added to the procedure as described previously (18,19). Subsequently, endpoints of previously performed ablations were verified and completed if necessary.

Offline HDM analysis

Maps were analyzed offline after the procedures using a non-commercial version of the Rhythmia™ software. Lumipoint™ algorithms were applied. These included the 'activation search' feature (highlighting regions of the map which contain electrograms that show activity in the time-of-interest), the 'complex activation' feature (highlighting regions of the map that both activate within the time-of-interest period and exhibit multiple components of activation), the 'Skyline graph' feature (reflecting the size of the depolarizing region throughout the mapping window), the 'split activation' feature (highlighting areas of the map that exhibit discontinuous activation), as well as the 'trend tool' (a visualization concept aiming to identify gaps in lines). Lumipoint™ confidence was applied aiming to estimate the likelihood or probability of an electrogram having a genuine biological activation at a particular point in time.

Follow-up

Patients underwent outpatient clinical visits 3 to 6 months after ablation. Pacemaker and implantable cardioverter-defibrillator were followed up through remote monitoring. 12-channel-electrocardiograms (ECGs) as well as 24-hour Holter ECGs were conducted in all patients without implantable devices. Any recurrence of arrhythmia >30 seconds during Holter ECG or registration of atrial high-rate episodes in patients with implantable devices were regarded as a recurrence (20). Additional outpatient clinical visits were conducted whenever symptomatic episodes

occurred suggestive of arrhythmia recurrence or in case of a deteriorated clinical condition of the patient.

Statistical analysis

All continuous variables were tested for normal distribution using the Shapiro-Wilk test. Parametric data are expressed as mean \pm standard error of the mean, whereas results of non-parametric data are provided as medians with interquartile ranges (IQR). If applicable, minimum and maximum values are also indicated. All analyses were performed using Graphpad Prism 8[®] (Graphpad Inc., La Jolla, CA, USA) and Microsoft Excel. For calculation of differences of continuous data between the CHD group of moderate and great complexity, the Mann-Whitney U test was used. A P value <0.05 was considered statistically significant.

Results

Patient characteristics

We studied data from 19 consecutive adult patients with CHD (53 ± 3 years; 10 male; $n=14$ with previous cardiac surgery/ $n=12$ with catheter ablation procedures) and an indication for catheter ablation of cardiac arrhythmias. Detailed patient characteristics are presented in *Table 1*. CHD conditions consisted of patients with moderate complexity in 15 (79%) and great complexity in 4 patients (21%). A detailed overview including underlying CHD and current ACHD AP classification, previous interventions and detected arrhythmia is presented in *Table 2*. Atrial tachycardia (AT) was diagnosed in 10 patients (53%) and atrial fibrillation (AF) in 7 patients (37%). Atrioventricular reentrant tachycardia was detected in 1 patient (5%). Ventricular arrhythmias were observed in 3 patients (16%) [frequent premature ventricular contractions: $n=1$; ventricular tachycardia (VT): $n=2$]. Reduced left ventricular ejection fraction was detected in 5 patients (26%), of which 3 presented with CHD of great complexity.

Procedural characteristics

Detailed procedural characteristics sorted by ablation conducted and CHD complexity are shown in *Tables 3* and *4*. In total, 21 procedures were conducted with a mean procedural time of 189 ± 23 minutes, mean fluoroscopy

time of 23 ± 4 minutes and a mean area dose product of 992 ± 279 cGym². Eleven out of 21 procedures (52%) displayed a re-do catheter ablation (AF: $n=5$; AT: $n=3$; VT: $n=2$; atrioventricular node ablation: $n=1$). Moreover, one patient with a history of CTI ablation presented for first-time AF ablation (*Table 2*, No. 4).

At the beginning of 15 procedures, sinus rhythm or intermittent/permanent pacemaker stimulation were present (67%; supraventricular $n=11$; ventricular $n=4$) with subsequent arrhythmia induction during these procedures in all but 2 patients who underwent atrial fibrillation ablation. Clinical arrhythmia was present at the beginning of the electrophysiological study in 6 procedures (29%). Non-inducibility of stable AT was accomplished in 7 out of 11 procedures. In ventricular tachycardia ablation, non-inducibility was reached in 1 out of 3 procedures, respectively. No arrhythmia induction attempt was performed after ablation in one procedure of AT and VT ablation each due to poor hemodynamic toleration and advanced procedure duration, whereas ablation of the critical isthmus based on activation and voltage map was successful with consecutive arrhythmia termination.

Acute procedural success was reached in all but one patient. In 1 patient with an Ebstein's anomaly (*Table 2*, No. 11), severely enlarged right atrium (volume: 257 mL) and moderate tricuspid insufficiency, postprocedural monitoring on the intensive care unit was initiated after beginning cardiac decompensation. This patient fully recovered rapidly without prolonged hospitalization. Another patient experienced retroperitoneal and scrotal hemorrhage after VT ablation and received successful conservative treatment. No other periprocedural complications occurred.

3-D electroanatomical high-density mapping and ablation

In total, 56 complete electroanatomical high-density maps with a median number of 11,073 (IQR, 5,217–16,593) mapping points per map were generated. Per procedure 1–4 critical areas were defined which were treated with 21 (IQR, 11–45) radiofrequency energy applications within a median ablation time of 16 (IQR, 12–45) minutes.

Atrial tachycardia ablation

In 11 procedures with AT, 19 activation maps were completed during arrhythmia with a range of 1–3 reentry circuits per procedure. Baseline AT cycle length in these

Table 1 Patient characteristics

Characteristics	Outcome
Baseline parameters, n=19	
Age (years)	53±3
Male sex, n [%]	10 [53]
BMI (kg/m ²)	27±1
Documented arrhythmias, n [%]	
Atrial fibrillation	7 [37]
Atrial tachycardia	10 [53]
AVRT	1 [5]
PVC	1 [5]
Ventricular tachycardia	2 [11]
Period known with arrhythmia (years)	
Atrial fibrillation	11.7±2.8
Atrial tachycardia	5.5 [1.5–13.5]
AVRT	0.04
PVC	0.4
Ventricular tachycardia	7 [4–14]
Patients with previous catheter ablation, n [%]	12 [63]
Number of previous catheter ablations per patient, n=12	2 [1–2]
Patients with previous cardiac surgery, n [%]	14 [74]
Number of previous surgeries per patient, n=13*	1 [1–2]
Devices, n [%]	
Pacemaker	3 [16]
2-lead ICD	2 [11]
CRT-D	1 [5]
CHD complexity score, n [%]	
Moderate complexity	15 [79]
Great complexity	4 [21]
Left ventricular ejection fraction, n [%]	
Normal (LVEF >50%)	12 [63] (range: 68–52)
Mildly impaired (LVEF 50–41%)	2 [11] (range: 50–41)
Moderately/highly impaired (LVEF <41%)	5 [26] (range: 35–18)

Table 1 (continued)**Table 1** (continued)

Characteristics	Outcome
Medication, n [%]	
Beta blocker	13 [68]
Class-Ic-AAD	1 [5]
Class-III-AAD	7 [37]
Oral anticoagulation	10 [53]
Rivaroxaban	4 [21]
Apixaban	3 [16]
Vitamin-K antagonist	4 [21]
Aspirin	4 [21]

Values are reported as mean ± s.e.m. or absolute numbers and percentages. In case of non-parametric data, results were provided as medians with interquartile ranges. *, the number of previous cardiac surgeries remained unclear in one patient. AAD, anti-arrhythmic drug; AVRT, atrioventricular reentry tachycardia; BMI, body mass index; CHD, congenital heart disease; CRT-D, cardiac resynchronization therapy with a built-in defibrillator; ICD, implantable cardioverter-defibrillator; LVEF, left ventricular ejection fraction; PVC, premature ventricular contraction.

patients was 301±22 ms (total range, 210–470 ms). AT mechanisms displayed as following: Localized reentry was detected in 3 (27%) and macroreentry in 7 AT procedures (64%) (*Figure 2*), whereas focal AT was present in 1 procedure (9%) (*Figure 3*). Critical AT arrhythmia substrate was detected in the left atrium in 6 (55%) and in the right atrium in 5 procedures (45%). Critical sites were distributed among the left atrium (roof: n=2; left pulmonary veins: n=1; mitral anulus: n=1; ridge: n=1; systemic venous antrum: n=1), whereas the majority of sites were located at the free wall (n=3; 75%) in the right atrium. Ablation resulted in acute successful arrhythmia termination in 10 out of these initial procedures. In one patient with transposition of the great arteries and previous Mustard procedure (*Table 2*, No. 17), no critical arrhythmic site of the clinically predominant tachycardia was detected in the left atrium while transbaffle puncture (suspected right atrial origin) was initially disapproved by this patient. After recurrence of arrhythmia during a follow up of 97 days, the patient approved inferior transbaffle puncture. Ablation of 3 ATs was conducted in the antero-lateral systemic as well as pulmonary atrium with successful acute termination and freedom from any arrhythmia during a 3

Table 2 Congenital heart diseases, previously conducted interventions and current arrhythmia

No.	CHD	ACHD AP classification	Previous surgical treatment	Previous catheter ablation	Current arrhythmia	AAD treatment
Moderate complexity						
1.	ASD secundum type	II C	–	–	AVRT	Beta-blocker
2.	ASD secundum type	II D	–	AVN ablation	Permanent AF	Amiodarone, beta-blocker
3.	ASD secundum type	II C	ASD repair*	–	Right AT	Amiodarone, beta-blocker
4.	APVC, ASD	II D	ASD and APVC repair	CTI ablation	AF	–
5.	APVC, ASD, COA	II C	ASD and APVC repair	CTI ablation	CTI-dependent atrial tachycardia	Beta-blocker
6.	APVC	II C	–	PVI, CTI, AT ablation	AF, left AT	Amiodarone
7.	BAV	II C	AVR, ascending aorta replacement, left atrial appendage resection, PVI	PVI	AF	Beta-blocker
8.	BAV	II C	–	PVI, CTI ablation	AF, left AT	Amiodarone, beta-blocker
9.	COA, BAV	II C	COA repair, aortic stent implantation	–	AF	Propafenone
10.	COA	II C	Aortic stent implantation	PVI, defragmentation, MIG-line	AT	Amiodarone, beta-blocker
11.	Ebstein's anomaly (no ASD)	II C	TVR, right atrial accessory AV-pathway ablation	Right incisional AT ablation	Right focal AT	Beta-blocker
12.	ToF	II C	ASD patch, PVR	PVI	AF	Beta-blocker, amiodarone
13.	ToF	II C	ToF repair, PVR	VT, CTI ablation	Left AT	Beta-blocker
14.	ToF	II C	PVR, VSD repair	–	PVCs	–
15.	ToF, APVC, unroofed coronary sinus, sinus venosus defect	II C	ToF repair, PVR, LSPV to right atrium anastomosis, RVOT dilatation)	–	Right AT	–
Great complexity						
16.	DORV	III D	DORV correction, patch enlargement	VT ablation	VT	Amiodarone, beta-blocker
17.	TGA	III D	Mustard procedure	–	Left AT	Sotalol
18.	TGA, dextrocardia	III C	Rashkind procedure, Senning procedure, pulmonary vein dilatation	–	Left AT	Beta-blocker
19.	ccTGA, VSD, bicuspid pulmonary valve, dextrocardia	III C	–	–	VT	Beta-blocker

*, surgery was conducted 6 months prior to catheter ablation after detection of pulmonary hypertension and arrhythmia. AAD, anti-arrhythmic drug; AF, atrial fibrillation; APVC, anomalous pulmonary venous connection; ASD, atrial septal defect; AT, atrial tachycardia; AVN, atrioventricular node; AVR, aortic valve replacement; AVRT, atrioventricular re-entry tachycardia; BAV, bicuspid aortic valve; ccTGA, congenitally corrected transposition of the great arteries; COA, coarctation of the aorta; CTI, cavotricuspid isthmus; DORV, double-outlet right ventricle; LSPV, left superior pulmonary vein; PVC, premature ventricular contraction; PVI, pulmonary vein isolation; PVR, pulmonary valve replacement; RVOT, right ventricular outflow tract; TGA, transposition of the great arteries; ToF, tetralogy of Fallot; TVR, tricuspid valve replacement; VSD, ventricular septal defect; VT, ventricular tachycardia.

Table 3 Procedural data sorted by ablation conducted

Procedural parameters	PVI	Defragmentation	AT ablation	VT ablation
Number of procedures, n	6	5	11	3
Baseline rhythm, n (%)				
Sinus rhythm	2 [33]	1 [20]	7 [64]	3 [100]
AF	3 [50]	2 [40]	0 [0]	0 [0]
AT	1 [17]	1 [20]	3 [27]	0 [0]
Partial/complete pacemaker-stimulation	0 [0]	1 [20]	1 [9]	2 [67]
Mapping and ablation data				
Re-do procedure, n (%)	5 [83]	3 [60]	2 [18]	2 [67]
Procedure time (min)	156 [119–186]	160 [135–189]	139±9	373 [349–500]
Fluoroscopy time (min)	19 [16–24]	19 [14–27]	13±2	49 [39–86]
Dose area product (cGym ²)	508 [387–819]	544 [470–774]	434±80	3,711 [2,035–5,240]
Mapping time (min)	20 [15–22]	17 [9–21]	23±3	98 [92–103]
Mapping points per map, n	11,028 [3,648–24,069]	5,975 [2,432–15,463]	12,848±2,406	10,205 [4,183–20,514]
Total radiofrequency applications*, n	50 [17–111]	54 [22–90]	11 [10–23]	44 [15–72]
Total radiofrequency duration* (min)	35 [11–60]	51 [27–59]	14 [8–19]	59 [12–70]
Chamber volumes given by mapping system (mL)				
Left atrial volume	151 [115–161]	147 [125–162]	119 [80–149]	–
Right atrial volume	–	–	145 [85–191]	–
Left ventricular volume	–	–	–	182 [108–215]
Right ventricular volume	–	–	–	119 [96–142]

Values are reported as mean ± s.e.m. or absolute numbers and percentages. In case of non-parametric data, results were provided as medians with interquartile ranges. *, radiofrequency applications and duration include all further ablation after AT termination (pulmonary vein re-isolation, completion of lines). AF, atrial fibrillation; AT, atrial tachycardia; PVI, pulmonary vein isolation; VT, ventricular tachycardia.

month follow-up period.

Atrial fibrillation ablation

AF ablation was performed in 7 procedures (33%), where partial or complete reconnection of pulmonary veins after previous PVI was detected in 6 patients [left pulmonary veins: n=3 (50%); right pulmonary veins: n=5 (83%)]. Ablation of complex fractionated atrial electrograms (CFAE) was conducted in 5 procedures (CFAE ablation only due to isolated pulmonary veins: n=1; CFAE + re-do PVI: n=4) and a re-do PVI only in 2 procedures. A total of 20 CFAE sites were registered (3.3±1.1 per procedure) equally distributed

among the left atrium (roof: n=4; anterior wall: n=3; septal wall: n=3; lateral wall: n=1; inferior wall: n=2; posterior wall: n=2; ridge/left atrial appendage: n=4 coronary sinus: n=1). Catheter ablation resulted in AF termination in 6 patients, with 1 patient receiving subsequent amiodarone application and electrocardioversion for sinus rhythm restitution.

Ablation of ventricular tachycardia and premature ventricular contractions

A total number of 3 VT procedures were conducted in 2 patients (Table 2, No. 16 and No. 19; Figure 4A). Overall, 7 morphologies were registered with a median VT

Table 4 Procedural data sorted by complexity of the CHD

Procedural parameters	Moderate complexity	Great complexity
Ablation conducted		
Number of procedures, n	16	5
Re-do procedure, n [%]	9 [56]	2 [40]
PVI, n [%]	6 [38]	0 [0]
Defragmentation, n [%]	4 [25]	0 [0]
AT ablation, n [%]	9 [56]	2 [40]
AV-Node ablation, n [%]	1 [6]	0 [0]
AVRT ablation, n [%]	1 [6]	0 [0]
PVC ablation, n [%]	1 [6]	0 [0]
VT ablation, n [%]	0 [0]	3 [60]
Baseline rhythm, n [%]		
Sinus rhythm	9 [56]	4 [80]
AF	4 [25]	0 [0]
AT	2 [13]	0 [0]
Partial/complete pacemaker-stimulation	1 [6]	1 [20]
Mapping and ablation data		
Procedure time (min)	150 [126–181]	349 [138–437]
Fluoroscopy time (min)	18±1	39 [7–67]
Dose area product (cGym ²)	470 [366–760]	2,035 [177–4,475]
Mapping time (min)	19 [10–23]	92 [28–100]
Mapping points per map, n	11,707±2,091	10,205 [5,443–16,228]
Total RF applications*, n	21 [10–43]	23 [11–58]
Total RF duration* (min)	19±5	22 [10–64]
Chamber volumes given by mapping system (mL)		
Left atrial volume	132±11	85 [54–115]
Right atrial volume	156 [100–188]	70 [#]
Left ventricular volume	165 [#]	182 [108–215]
Right ventricular volume	30 [#]	119 [96–142]

Values are reported as mean ± s.e.m. or absolute numbers and percentages. In case of non-parametric data, results were provided as medians with interquartile ranges. *, radiofrequency applications and duration include all further ablation after AT termination (pulmonary vein re-isolation, completion of lines); #, only one value was available for this parameter. AF, atrial fibrillation; AT, atrial tachycardia; AV, atrioventricular; AVRT, atrioventricular reentrant tachycardia; PVC, premature ventricular contraction; PVI, pulmonary vein isolation; RF, radiofrequency; VT, ventricular tachycardia.

cycle length of 380 (IQR, 345–400) ms and consecutive completion of 7 maps (right ventricle: n=1; left ventricle: n=6). Ablation resulted in successful clinical VT termination in both patients. In one patient with surgically

treated tetralogy of Fallot (*Table 2*, No. 14), frequent premature ventricular contractions were addressed in 2 localizations (left ventricular apex, ventricular outflow tract).

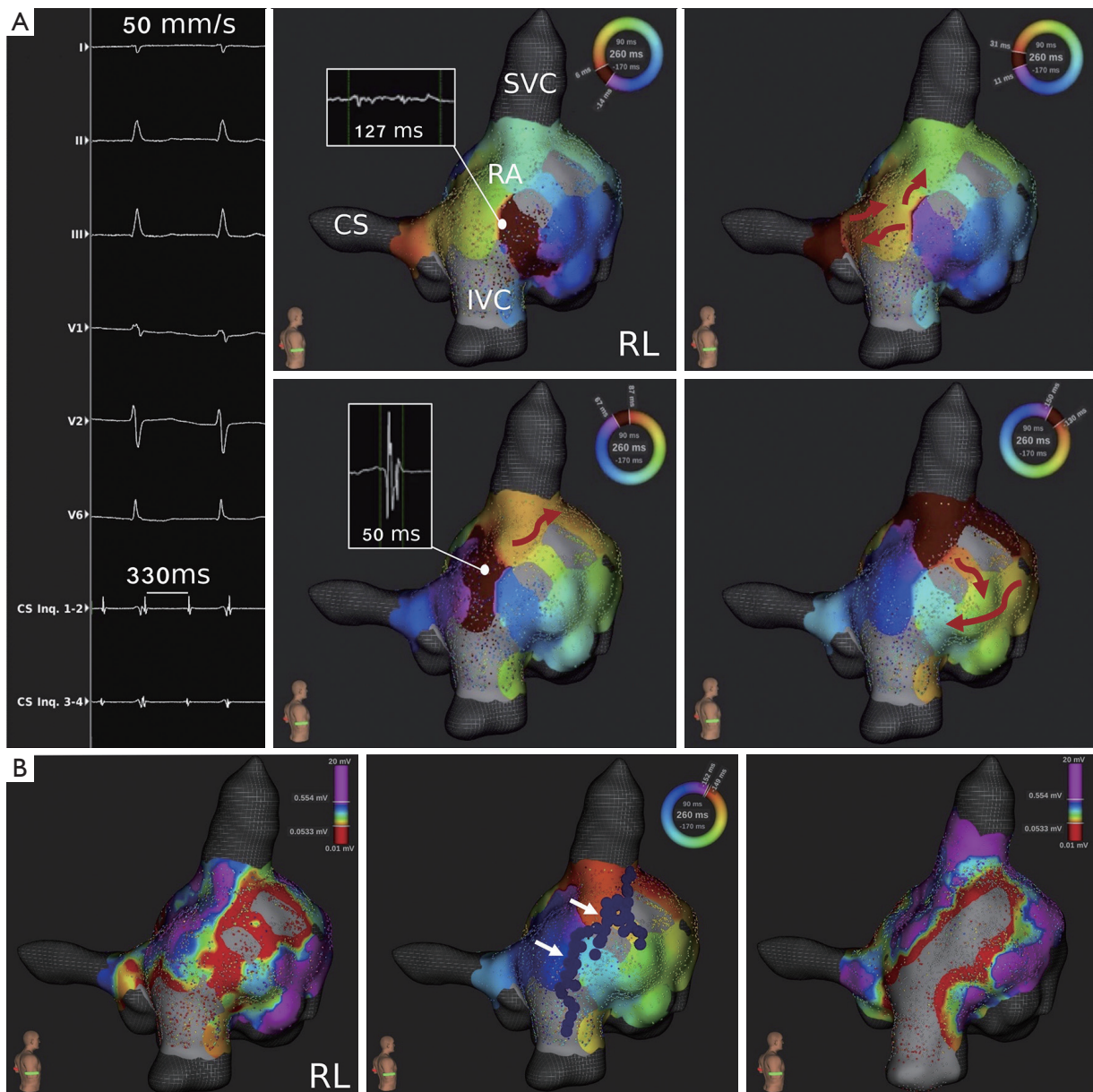


Figure 2 Lateral wall circuit in a right atrial macroreentrant tachycardia. (A) Critical isthmus detection (upper right figure) at the lateral wall of the right atrium during macroreentrant atrial tachycardia in a patient with surgically corrected tetralogy of Fallot. Activation maps acquired by HDM visualize slow conduction zones of up to 127 ms (upper left figure) which enabled macroreentrant circulation (red arrows) at a cycle length of 330 ms (CS electrogram recordings on the left) around the scar areas (grey). Wavefront collision is observed afterwards as the electrogram shows multiple deflections and low fractionation (lower left figure). (B) Activation and voltage maps before and after successful isthmus ablation. Large, discontinuous low voltage areas are detected (left figure, red areas). No-voltage areas were connected and critical isthmus sites were dissolved following linear ablation between the superior and inferior vena cava (SVC/IVC) (middle figure, white arrows mark the ablation area; right figure, grey area marks the dissolved isthmus). Additional CTI ablation was performed afterwards. CS, coronary sinus; CTI, cavotricuspid isthmus; IVC, inferior vena cava; RA, right atrium; RL, right lateral view; SVC, superior vena cava.

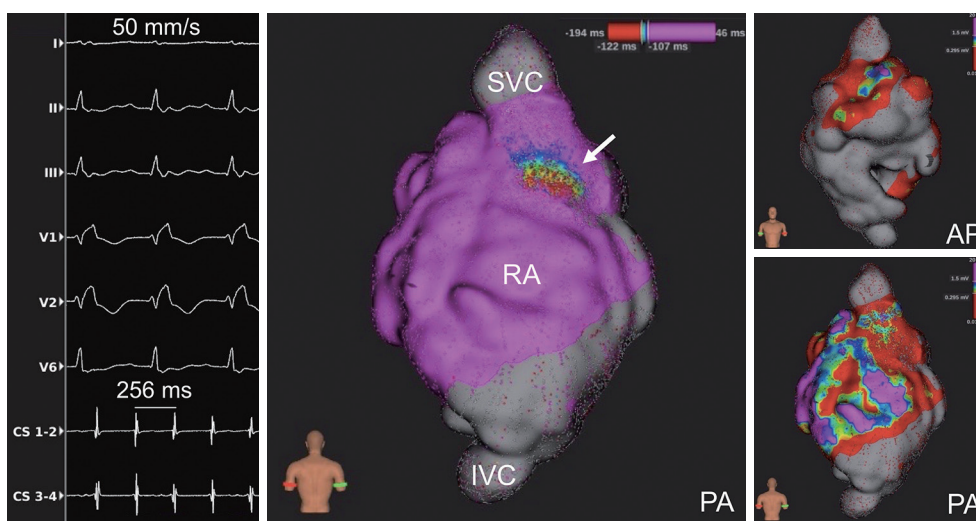


Figure 3 HDM of focal atrial tachycardia in a patient with Ebstein's anomaly. The surface ECG and coronary sinus (CS) tracings (left figure) show an atrial tachycardia cycle length of 256 ms. After HDM during arrhythmia, early activation of the ectopic area is visible (white arrow). According voltage maps (right figures) show large low voltage areas in the posterior as well as anterior right atrium, indicating scarring after cardiac surgery. Note the severely enlarged right atrium of 257 mL. AP, anterior posterior view; HDM, high-density mapping; IVC, inferior vena cava; PA, posterior-anterior view; RA, right atrium; SVC, superior vena cava.

Postprocedural signal processing

Postprocedural signal processing using Lumipoint™ allowed automated annotation of fractionated signals within specific windows of interest supporting arrhythmia mechanism characterization and identification of critical isthmus sites. Independent of activation time annotation, the 'activation search' feature identified the isthmus where the automatically annotated map did not clearly indicate it (Figure 4B). The 'complex activation search' feature identified a subset of late potentials with fractionated signals during substrate mapping in all patients undergoing VT ablation (Figure 4C). Overall, Lumipoint™ successfully displayed critical isthmus sites in 10 out of 15 procedures (67%) and 20 out of 27 completed AT, atrioventricular reentrant tachycardia and VT maps (74%).

Postprocedural signal processing could not be applied due to subsequent partial (n=1) or complete (n=2) arrhythmia mapping using the ablation catheter in 3 out of 15 procedures (20%). Moreover, critical isthmus detection using Lumipoint™ was not possible in 2 out of 15 procedures (13%) with microreentrant AT and intermittent AF. In both procedures, postprocedural signal processing using Lumipoint™ was not applicable due to repeatedly occurring rapid degeneration of AT into AF, which consecutively lead to incomplete generation of activation

maps during the clinically relevant AT. Nevertheless, ablation guided by middiastolic low amplitude fractionated signals resulted in acute success in both procedures.

Using the 'split activation' and 'trend tool' feature, gap confirmation in a previously set CTI ablation line was successful in a patient with recurrent CTI-dependent macroreentrant AT (Table 2, No. 5; Figure 5). Two right-atrial accessory pathways were also displayed by activation mapping including the Lumipoint™ software and successfully treated in a patient with atrioventricular reentrant tachycardia (Table 2, No. 1).

Follow-up

Acute procedural success was achieved in all but one patient. One patient was lost during follow-up due to a considerable distance to the patient's residence. During a median follow-up time of 140 (IQR, 91–190) days, recurrence of AF/AT/VT after a single HDM-guided procedure occurred in 4, 4, and 2 patients, respectively. Two out of these patients with AF/AT showed different arrhythmias (compared with the initial HDM-guided procedure) at follow-up. When comparing patients with CHD of moderate and great complexity, no statistically significant difference regarding arrhythmia recurrence was registered between both groups [n=6 (40%) vs. n=4 (100%); P=0.09].

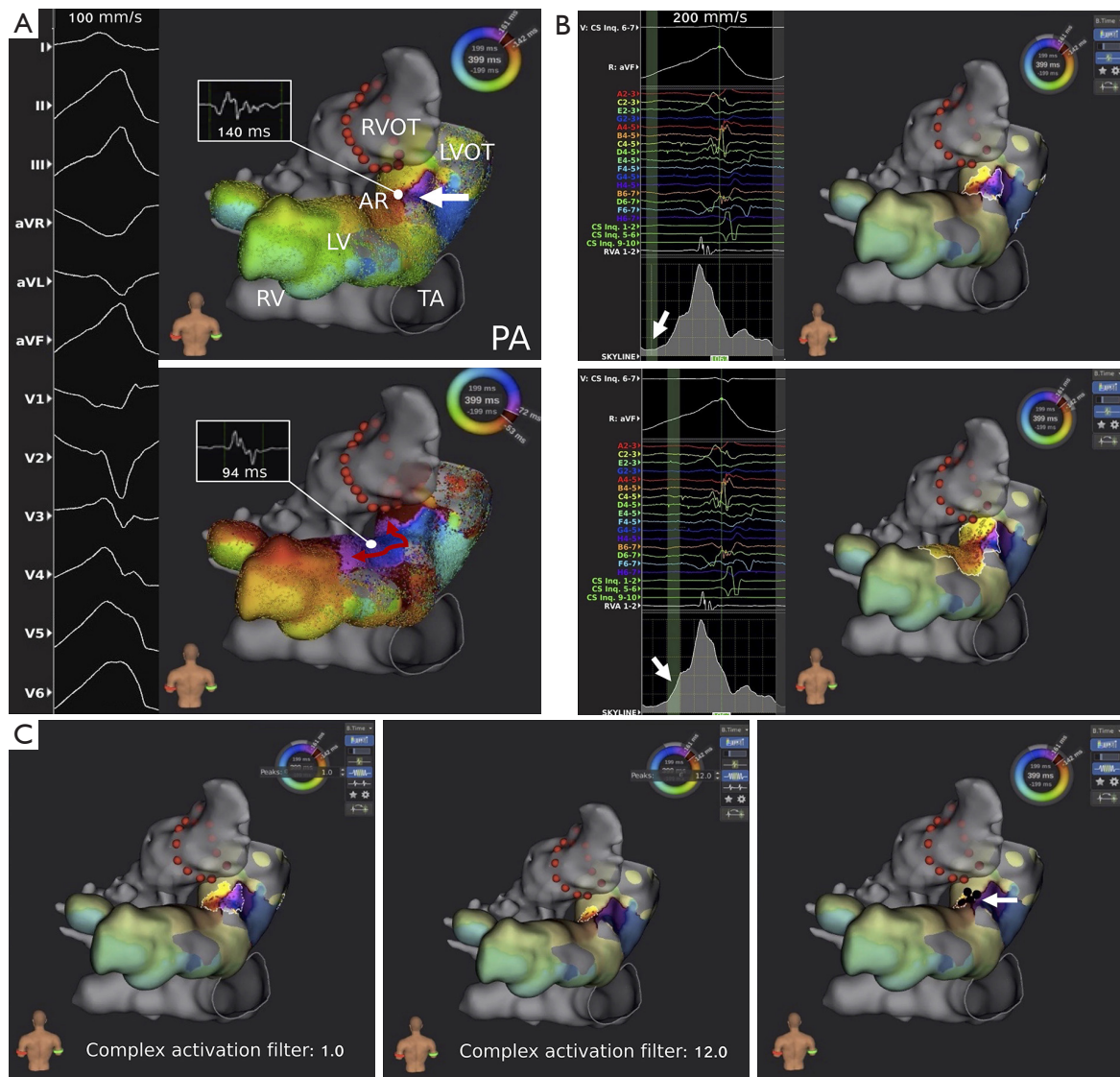


Figure 4 Lumipoint™ postprocedural signal processing during macroreentrant ventricular tachycardia. (A) Activation maps of the left (LV) and anatomic map of the right ventricle (RV) with the according 12-channel ECG in a patient with surgically corrected double-outlet right ventricle and recurrent ventricular tachycardia. The 12-lead ECG tracings indicate a left ventricular outflow tract (LVOT) origin. Acquired high-density maps showed slow conduction and severe fractionation of up to 140 ms (upper figure, white arrow) in the area of the aortic root (AR), indicating a possible critical isthmus area (lower figure). (B) Postprocedural signal processing and critical isthmus detection using the 'skyline' graph and 'activation search' feature. Simultaneous area activation is highlighted in the activation map independent of activation time annotation. The point of fewest overall depolarization reflects the critical isthmus which can be detect by selecting the lowest skyline graph value ('skyline valley') within the window of interest (upper figure, green highlighted and marked by the white arrow). The window of interest was selected as 10% of the reentry circuit cycle length (40 ms). In the associated Lumipoint™ activation map, the critical isthmus area is visualized (upper figure, white bordered area). Rapid depolarization of adjacent myocardium followed afterwards (lower figure, white bordered area) which is displayed in the skyline graph as a steep slope increase (lower figure, white arrow). (C) Identification of late potentials with fractionated signals using the 'complex activation' search feature. The 'complex activation' filter is applied for localization of potentials with severe fractionation (left figure: peak filter at 1.0; middle figure: peak filter at 12.0; white bordered area displays fractionated signals). The area of severe fractionation was ablated subsequently (right figure, black points marked by the white arrow) and resulted in arrhythmia termination. AR, aortic root; LV, left ventricle; LVOT, left ventricular outflow tract; PA, posterior-anterior view; RV, right ventricle; RVOT, right ventricular outflow tract; TA, tricuspid annulus.

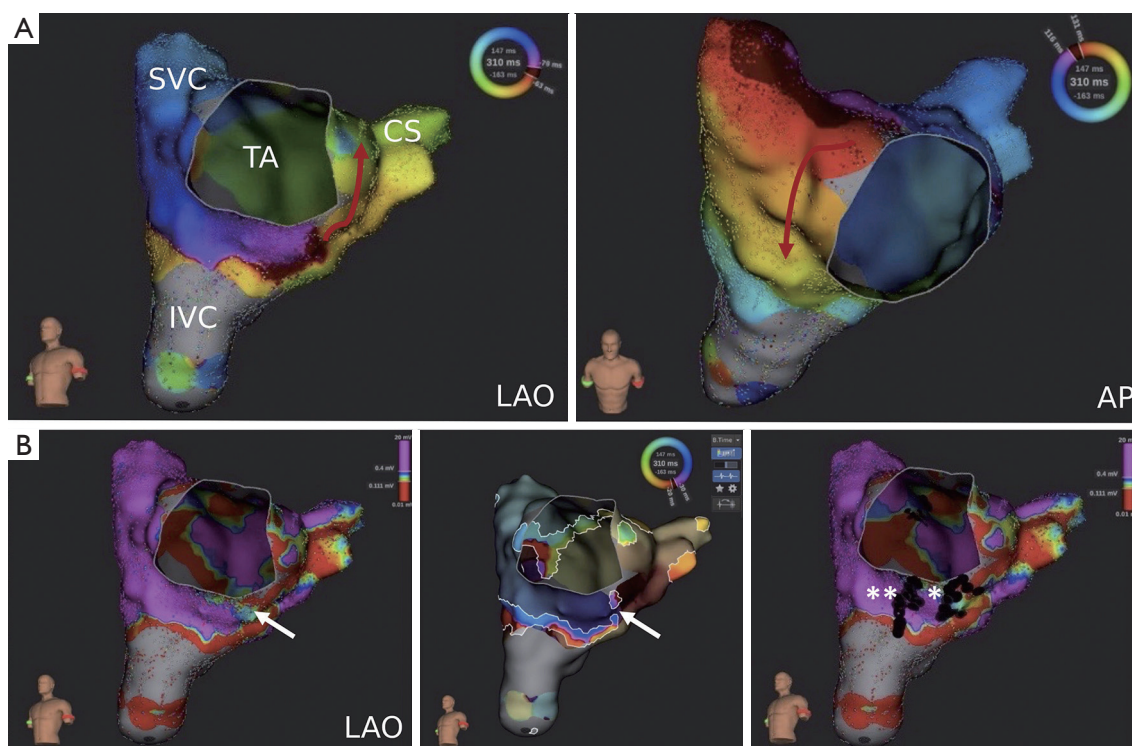


Figure 5 HDM and postprocedural signal processing of macroreentrant right atrial tachycardia. (A) The macroreentrant circuit around the tricuspid annulus (TA) is visualized in the activation map (left and right figure). (B) In the corresponding voltage map, a gap was suspected in the area of previous cavotricuspid isthmus (CTI) ablation (left figure, white arrow). Postprocedural signal analysis using the Lumipoint™ ‘split activation’ feature confirms the gap (middle figure, white arrow). Completion of the initial lesion set (right figure, marked by white *) only resulted in an unidirectional block. A second, more lateral new linear ablation (marked by white **) resulted in a successful bidirectional CTI block. AP, anterior posterior view; CS, coronary sinus; CTI, cavotricuspid isthmus; LAO, left anterior oblique view; HDM, high-density mapping; IVC, inferior vena cava; TA, tricuspid annulus.

For treatment of recurrent arrhythmia, 4 patients received an antiarrhythmic drug treatment only [beta-blocker: n=4 (100%); flecainide: n=1 (25%)]. An additional ablation procedure was conducted in 6 patients (AF: n=2; AT: n=3; VT: n=1) within a median time of 176 (IQR, 73–313) days between both procedures. Five out of these 6 patients showed freedom of arrhythmia after a second HDM-guided ablation procedure, with one patient showing recurrence of AF. No long-term complications were observed in all patients.

Discussion

The present findings suggest that HDM of cardiac arrhythmias can provide detailed insights into arrhythmia substrate and mechanisms. Acquired maps reflected underlying arrhythmogenic substrates with high spatial

resolution and allowed target-orientated activation mapping of complex focal as well as macro- and microreentrant arrhythmias. Additionally, novel automated annotation algorithms supported rapid identification of regions critical for arrhythmia preservation. This might facilitate catheter ablation in patients with moderate to great CHD.

The role of catheter ablation in CHD

Supraventricular as well as ventricular tachycardias are a leading cause of hospitalization and predictor of mortality in patients with CHD (21,22). Especially in patients with CHD and pulmonary arterial hypertension, occurrence of supraventricular arrhythmia may be regarded as a progression of hemodynamic deterioration (23). Antiarrhythmic drug management is often limited in CHD, as it is mostly adapted from clinical studies conducted

in patients with acquired heart diseases. No randomized controlled trials are available for specific guidance of antiarrhythmic drug treatment due to the heterogeneity and continued evolution of CHD in adults (1). Beta-blockers are probably useful, while sotalol and amiodarone should be avoided—at least as first-intention treatment—because of the risk of proarrhythmia and potential long-term side effects (24–26). In line with recent international consensus, amiodarone may be considered for AF and AT recurrence prevention in patients with CHD and ventricular dysfunction, hypertrophy of systemic ventricle, or coronary artery disease, in whom catheter ablation fails or is otherwise no option. Class I antiarrhythmic drugs may be harmful in case of a diseased ventricle (26,27). Therefore, catheter ablation guided by electro-anatomical 3D-mapping is regarded as the first-line therapy and is preferred to long-term pharmacological treatment in CHD related arrhythmias whenever no reversible hemodynamic or other factors can be addressed (1).

Clinical implications of HDM in patients with CHD

Corrected anatomy after pediatric cardiac surgery, abnormal anatomical localization or disturbances within the conduction system and iatrogenic scarring can create complex arrhythmogenic substrate (28) while multiple arrhythmia mechanisms are frequently present in patients with CHD (26).

Conventional point-by-point 3D electro-anatomical mapping has been developed more than two decades ago and has been found to produce favorable outcome in CHD-related catheter ablation (6). However, the collection of even a few hundred points is time-consuming and still often need additional manual annotation. Moreover, the electrode size, spacing and design within most presently used single-tip catheters (in conjunction with classical signal to noise ratios within classical 3-D mapping algorithms) only show limited electrogram resolution and can be additionally limited by far-field signals (29).

Noteworthy, within the last 5 years HDM has been found to open up new avenues in the treatment of cardiac arrhythmias in a wide range of patients (30). HDM deepened our understanding of cardiac electrophysiology and arrhythmogenesis by rapid acquisition of thousands of activation points independent of activation time. Small and closely spaced electrodes enable characterization of arrhythmogenic substrate with high spatiotemporal

resolution. The low noise level (0.01 mV) allows registration of electrograms with very low amplitude, which for instance can improve identification of reconnection gaps in pulmonary veins (31) or concealed low voltage propagation within the pulmonary vein antra (32) in patients with AF. Moreover, HDM can enhance the precise display of complex arrhythmia mechanisms in atrial as well as ventricular tachycardia (8,33). It becomes now evident that multiple isthmus, double-loop and localized reentries are more frequently present than previously thought (34,35). This is of importance as HDM can indicate conduction and substrate variability where long post-pacing intervals during entrainment alone can be misleading (19,30). HDM furthermore supports fast arrhythmogenic substrate characterization in patients with either hemodynamically not tolerated, non-inducible or short lasting episodes of VT (9,15), as pacemapping of VT circuits can be aggravated in case of multiple entrances and exits (8).

And entrainment mapping alone can overestimate isthmus dimensions in some cases (36).

As a result, several HDM guided ablation strategies aiming to avoid extensive radiofrequency current delivery and minimize the risk of a stiff left atrial syndrome have been proposed (37). These recent developments have also been found to be useful in the treatment of patients with CHD, but have only been reported in a limited number of patients (12,38). Not surprisingly, the here presented data also show that arrhythmia-free survival following HDM-guided ablation is not guaranteed. Therefore, further studies are needed to investigate long-term efficacy.

Safety

HDM has been found to result in similar safety in comparison to classical point-by-point mapping in various settings (9,18). The recently published TRUE HD prospective multicenter study (39) as well as smaller studies (40) confirmed acute safety, effectiveness and feasibility of HDM for catheter ablation of a wide spectrum of arrhythmias. Device-related serious adverse events were reported to be 0.57–1.25% (39,40) and might be even lower as supported by our experience from more than 500 procedures. Our findings regarding radiation exposure and safety outcome were comparable to previously published studies having used conventional point-by-point mapping in adult patients with different CHD-related arrhythmias (41,42).

Lumipoint™ algorithm

The Lumipoint™ automated annotation algorithm may enhance interpretation, detection and ablation of complex arrhythmogenic substrate using the following features: First, the ‘activation search’ feature highlights areas with simultaneous depolarization in the activation map independent of activation time annotation. As annotation of single activation signals may be insufficient at sites with complex multiple fractionation of signals (43), demarcation of multiple simultaneously activated regions can improve the characterization of complex arrhythmogenic substrate and potential arrhythmia-maintaining regions. Moreover, farfield signals can be automatically annotated by the algorithm, consecutively improving ablation guidance (44). Second, the area of fewest overall depolarized tissue can be marked by using the skyline feature (‘skyline valley’) within a window of interest, which displays the critical isthmus of AT or VT circuits (44,45). As standardized approaches for system adjustments of the different Lumipoint™ features are still to be developed, further studies are needed for optimized utilization of the Lumipoint™ algorithm.

Limitations

The present study has some limitations that need to be addressed. Most importantly, this is a single-center experience investigating the usefulness of novel automated annotation algorithms in a relatively small number of patients with CHD in a retrospective manner. Moreover, the current study does not compare the efficacy of HDM with conventional methods of mapping and ablation. Due to strict exclusion criteria about one-third of maps could not be used for postprocedural signal processing using Lumipoint in this patient series. This was mainly driven by incomplete activation mapping because of usage of the ablation catheter instead of the IntellaMap Orion™ catheter.

Conclusions

The findings of the present study suggest that HDM provides detailed insights into CHD-related arrhythmia substrate and mechanisms. In conjunction with novel automated annotation algorithms this might facilitate tailored catheter ablation in patients with moderate to great CHD complexity. Further studies are needed to assess long-term efficacy of HDM as a treatment modality of arrhythmias in CHD.

Acknowledgments

We thank Ms. Lydia Merbold for excellent technical assistance during ultra-high density mapping using the Rhythmia™ system and Lumipoint™ software application during ablation procedures and offline analysis.

Footnote

Conflicts of Interest: C Meyer: speaker for Boston Scientific and Abbott; consultant for Biosense Webster. The other authors have no conflicts of interest to declare.

Ethical Statement: The authors are accountable for all aspects of the work in ensuring that questions related to the accuracy or integrity of any part of the work are appropriately investigated and resolved. The study was approved by the local ethics committee of the University of Hamburg (No. WF-79/16) and informed consent was taken from all patients.

References

1. Hernández-Madrid A, Paul T, Abrams D, et al. Arrhythmias in congenital heart disease: a position paper of the European Heart Rhythm Association (EHRA), Association for European Paediatric and Congenital Cardiology (AEPC), and the European Society of Cardiology (ESC) Working Group on Grown-up Congenital Heart Disease, endorsed by HRS, PACES, APHRS, and SOLAECE. *Europace* 2018;20:1719-53.
2. Meyer C, Martinek M, Winter S, et al. Arrhythmias in patients with surgically corrected tetralogy of Fallot. *Herzschrittmacherther Elektrophysiol* 2010;21:189-95.
3. Stout KK, Daniels CJ, Aboulhosn JA, et al. 2018 AHA/ACC Guideline for the Management of Adults With Congenital Heart Disease. *Circulation* 2019;139:e637-97.
4. Maury P, Sacher F, Rollin A, et al. Ventricular arrhythmias and sudden death in tetralogy of Fallot. *Arch Cardiovasc Dis* 2017;110:354-62.
5. Triedman JK, Alexander ME, Love BA, et al. Influence of patient factors and ablative technologies on outcomes of radiofrequency ablation of intra-atrial re-entrant tachycardia in patients with congenital heart disease. *J Am Coll Cardiol* 2002;39:1827-35.
6. Delacretaz E, Ganz LI, Soejima K, et al. Multiple atrial macro-re-entry circuits in adults with repaired congenital heart disease: entrainment mapping combined with three-

- dimensional electroanatomic mapping. *J Am Coll Cardiol* 2001;37:1665-76.
7. Ueda A, Suman-Horduna I, Mantziari L, et al. Contemporary Outcomes of Supraventricular Tachycardia Ablation in Congenital Heart Disease: A Single-Center Experience in 116 Patients. *Circ Arrhythm Electrophysiol* 2013;6:606-13.
 8. Martin R, Maury P, Bisceglia C, et al. Characteristics of Scar-Related Ventricular Tachycardia Circuits Using Ultra-High-Density Mapping. *Circ Arrhythm Electrophysiol* 2018;11:e006569.
 9. Nühlich JM, Kaiser L, Akbulak RÖ, et al. Substrate characterization and catheter ablation in patients with scar-related ventricular tachycardia using ultra high-density 3-D mapping. *J Cardiovasc Electrophysiol* 2017;28:1058-67.
 10. Gunawardene M, Munkler P, Eickholt C, et al. A novel assessment of local impedance during catheter ablation: initial experience in humans comparing local and generator measurements. *Europace* 2019;21:i34-42.
 11. Kaiser L, Jularic M, Akbulak RÖ, et al. Catheter ablation of hemodynamically unstable ventricular tachycardia in ischemic cardiomyopathy using high-resolution mapping. *Clin Case Rep* 2017;5:389-93.
 12. Xue Y, Liu Y, Liao H, et al. Evaluation of Electrophysiological Mechanisms of Post-Surgical Atrial Tachycardias Using an Automated Ultra-High-Density Mapping System. *JACC Clin Electrophysiol* 2018;4:1460-70.
 13. Salukhe TV, Willems S, Drewitz I, et al. Propofol sedation administered by cardiologists without assisted ventilation for long cardiac interventions: an assessment of 1000 consecutive patients undergoing atrial fibrillation ablation. *Europace* 2012;14:325-30.
 14. Anter E, Tschabrunn CM, Contreras-Valdes FM, et al. Pulmonary vein isolation using the Rhythmia mapping system: Verification of intracardiac signals using the Orion mini-basket catheter. *Heart Rhythm* 2015;12:1927-34.
 15. Sultan A, Bellmann B, Luker J, et al. The use of a high-resolution mapping system may facilitate standard clinical practice in VE and VT ablation. *J Interv Card Electrophysiol* 2019. doi: 10.1007/s10840-019-00530-1.
 16. Schaeffer B, Hoffmann BA, Meyer C, et al. Characterization, Mapping, and Ablation of Complex Atrial Tachycardia: Initial Experience With a Novel Method of Ultra High-Density 3D Mapping. *J Cardiovasc Electrophysiol* 2016;27:1139-50.
 17. Shah D, Haissaguerre M, Takahashi A, et al. Differential pacing for distinguishing block from persistent conduction through an ablation line. *Circulation* 2000;102:1517-22.
 18. Rottner L, Metzner A, Ouyang F, et al. Direct Comparison of Point-by-point and Rapid Ultra High-Resolution Electroanatomical Mapping in Patients Scheduled for Ablation of Atrial Fibrillation. *J Cardiovasc Electrophysiol* 2017;28:289-97.
 19. Pathik B, Lee G, Sacher F, et al. New Insights Into an Old Arrhythmia: High-Resolution Mapping Demonstrates Conduction and Substrate Variability in Right Atrial Macro-Re-Entrant Tachycardia. *JACC Clin Electrophysiol* 2017;3:971-86.
 20. January CT, Wann LS, Calkins H, et al. 2019 AHA/ACC/HRS Focused Update of the 2014 AHA/ACC/HRS Guideline for the Management of Patients With Atrial Fibrillation: A Report of the American College of Cardiology/American Heart Association Task Force on Clinical Practice Guidelines and the Heart Rhythm Society. *J Am Coll Cardiol* 2019;74:104-32.
 21. Koyak Z, Harris L, De Groot JR, et al. Sudden Cardiac Death in Adult Congenital Heart Disease. *Circulation* 2012;126:1944-54.
 22. Verheugt CL, Uiterwaal CSPM, Van Der Velde ET, et al. The emerging burden of hospital admissions of adults with congenital heart disease. *Heart* 2010;96:872-8.
 23. Drakopoulou M, Nashat H, Kempny A, et al. Arrhythmias in adult patients with congenital heart disease and pulmonary arterial hypertension. *Heart* 2018;104:1963-9.
 24. Thorne SA, Barnes I, Cullinan P, et al. Amiodarone-Associated Thyroid Dysfunction : Risk Factors in Adults With Congenital Heart Disease. *Circulation* 1999;100:149-54.
 25. Moore BM, Cordina RL, McGuire MA, et al. Efficacy and adverse effects of sotalol in adults with congenital heart disease. *Int J Cardiol* 2019;274:74-9.
 26. Khairy P, Van Hare GF, Balaji S, et al. PACES/HRS Expert Consensus Statement on the Recognition and Management of Arrhythmias in Adult Congenital Heart Disease. *Heart Rhythm* 2014;11:e102-e65.
 27. Fish FA, Gillette PC, Benson DW. Proarrhythmia, cardiac arrest and death in young patients receiving encainide and flecainide. *J Am Coll Cardiol* 1991;18:356-65.
 28. Ernst S, Saenen J, Rydman R, et al. Utility of noninvasive arrhythmia mapping in patients with adult congenital heart disease. *Card Electrophysiol Clin* 2015;7:117-23.
 29. Acosta J, Penela D, Andreu D, et al. Multielectrode vs. point-by-point mapping for ventricular tachycardia substrate ablation: a randomized study. *Europace* 2018;20:512-9.

30. Meyer C. High-density mapping-based ablation strategies of cardiac rhythm disorders: the RHYTHMIA experience at new horizons. *Europace* 2019;21:iii7-10.
31. García-Bolao I, Ballesteros G, Ramos P, et al. Identification of pulmonary vein reconnection gaps with high-density mapping in redo atrial fibrillation ablation procedures. *Europace* 2018;20:f351-8.
32. Segerson NM, Lynch B, Mozes J, et al. High-density mapping and ablation of concealed low-voltage activity within pulmonary vein antra results in improved freedom from atrial fibrillation compared to pulmonary vein isolation alone. *Heart Rhythm* 2018;15:1158-64.
33. Mantziari L, Butcher C, Shi R, et al. Characterization of the Mechanism and Substrate of Atrial Tachycardia Using Ultra-High-Density Mapping in Adults With Congenital Heart Disease: Impact on Clinical Outcomes. *J Am Heart Assoc* 2019;8:e010535.
34. Takigawa M, Derval N, Maury P, et al. Comprehensive Multicenter Study of the Common Isthmus in Post-Atrial Fibrillation Ablation Multiple-Loop Atrial Tachycardia. *Circ Arrhythm Electrophysiol* 2018;11:e006019.
35. Takigawa M, Derval N, Frontera A, et al. Revisiting anatomic macroreentrant tachycardia after atrial fibrillation ablation using ultrahigh-resolution mapping: Implications for ablation. *Heart Rhythm* 2018;15:326-33.
36. Anter E, Tschabrunn CM, Buxton AE, et al. High-Resolution Mapping of Postinfarction Reentrant Ventricular Tachycardia. *Circulation* 2016;134:314-27.
37. Calkins H, Hindricks G, Cappato R, et al. 2017 HRS/EHRA/ECAS/APHRS/SOLAECE Expert Consensus Statement on Catheter and Surgical Ablation of Atrial Fibrillation. *Heart Rhythm* 2017;14:e275-444.
38. Ernst S, Cazzoli I, Guarguagli S. An initial experience of high-density mapping-guided ablation in a cohort of patients with adult congenital heart disease. *Europace* 2019;21:i43-53.
39. Hindricks G, Weiner S, McElderry T, et al. Acute safety, effectiveness, and real-world clinical usage of ultra-high density mapping for ablation of cardiac arrhythmias: results of the TRUE HD study. *Europace* 2019:655-61.
40. Lackermair K, Kellner S, Kellnar A, et al. Initial single centre experience with the novel Rhythmia(c) high density mapping system in an all comer collective of 400 electrophysiological patients. *Int J Cardiol* 2018;272:168-74.
41. Liang JJ, Frankel DS, Parikh V, et al. Safety and outcomes of catheter ablation for atrial fibrillation in adults with congenital heart disease: A multicenter registry study. *Heart Rhythm* 2019;16:846-52.
42. Anguera I, Dallaglio P, Macías R, et al. Long-Term Outcome After Ablation of Right Atrial Tachyarrhythmias After the Surgical Repair of Congenital and Acquired Heart Disease. *Am J Cardiol* 2015;115:1705-13.
43. Irie T, Yu R, Bradfield JS, et al. Relationship Between Sinus Rhythm Late Activation Zones and Critical Sites for Scar-Related Ventricular Tachycardia: Systematic Analysis of Isochronal Late Activation Mapping. *Circ Arrhythm Electrophysiol* 2015;8:390-9.
44. Martin CA, Takigawa M, Martin R, et al. Use of Novel Electrogram "Lumipoint" Algorithm to Detect Critical Isthmus and Abnormal Potentials for Ablation in Ventricular Tachycardia. *JACC Clin Electrophysiol* 2019;5:470-9.
45. Takigawa M, Martin CA, Derval N, et al. Insights from atrial surface activation throughout atrial tachycardia cycle length: A new mapping tool. *Heart Rhythm* 2019. doi: 10.1016/j.hrthm.2019.04.029.

Cite this article as: Alken FA, Klatt N, Muenkler P, Scherschel K, Jungen C, Akbulak RO, Kahle AK, Gunawardene M, Jularic M, Dinshaw L, Hartmann J, Eickholt C, Willems S, Stute F, Mueller G, Blankenberg S, Rickers C, Sinning C, Zengin-Sahm E, Meyer C. Advanced mapping strategies for ablation therapy in adults with congenital heart disease. *Cardiovasc Diagn Ther* 2019;9(Suppl 2):S247-S263. doi: 10.21037/cdt.2019.10.02